Supplement of Atmos. Chem. Phys., 22, 5157–5173, 2022
https://doi.org/10.5194/acp-22-5157-2022-supplement

Atmospheric Chemistry and Physics
Open Access
EGU

Supplement of

Top-down and bottom-up estimates of anthropogenic methyl bromide emissions from eastern China

Haklim Choi et al.

Correspondence to: Sunyoung Park (sparky@knu.ac.kr)

Potential source regions

The regional distribution of potential CH_3Br sources in East Asia was derived by applying a statistical analysis to the air mass trajectories that correspond to the enhancements of CH_3Br above baseline at Gosan during 2008–2019. Among the various trajectory-based statistical approaches, we applied a trajectory statistics method based on Seibert et al. (1994) to identify the potential sources of atmospheric pollutants (Reimann et al., 2004; Li et al., 2014). This method assumes that the concentration enhancement above baseline at the observation site is proportional to the average concentration of each grid cell through which the air mass has passed and the residence time that the air mass spends in each grid cell. Therefore, the residence-time-weighted mean concentration $\overline{C_{mn}}$ of a target compound in each grid on the domain can be calculated as follows:

$$\overline{C_{mn}} = \frac{\sum_i^M (\tau_{mni} c_i)}{\sum_i^M \tau_{mni}}, \quad \text{S(1)}$$

where m,n is a potential source region of CH_3Br - *m,n* are indices of a horizontal grid cell, *i* is the index of the trajectory and *M* is the total number of trajectories, C_i is the enhanced concentration of CH_3Br above baseline and τ_{mni} is the residence time that trajectory *i* spent over the grid cell *m,n* within the atmospheric boundary layer. The calculation of the residence time over each grid was accomplished using the method of Poirot and Wishinski (1986), which assumes that an air parcel travels linearly between two points at constant speed.

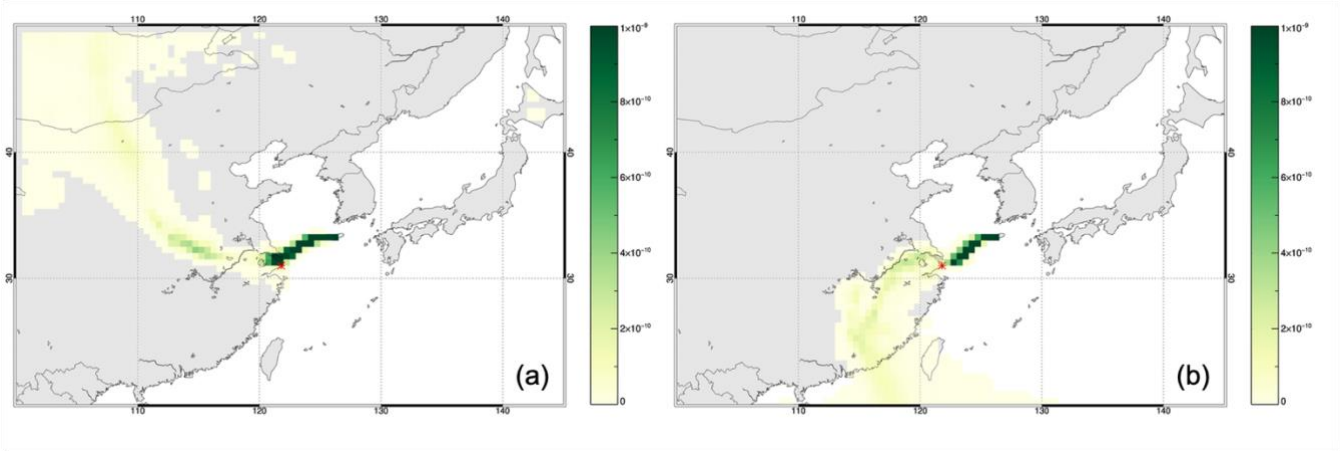

Figure S1: Spatial distributions of residence time simulated from the FLEXible PARTicle dispersion model (FLEXPART) (a) 12 UTC on 4 May 2016 and (b) 05 UTC on 4 January 2015. The Lagrangian back trajectories were computed for a large number of notional particles (n=50,000). The observed concentration of CH_3Br were (a) 41.2 ppt and (b) 25.3 ppt, respectively. The location of the port of Shanghai is marked with a red asterisk.

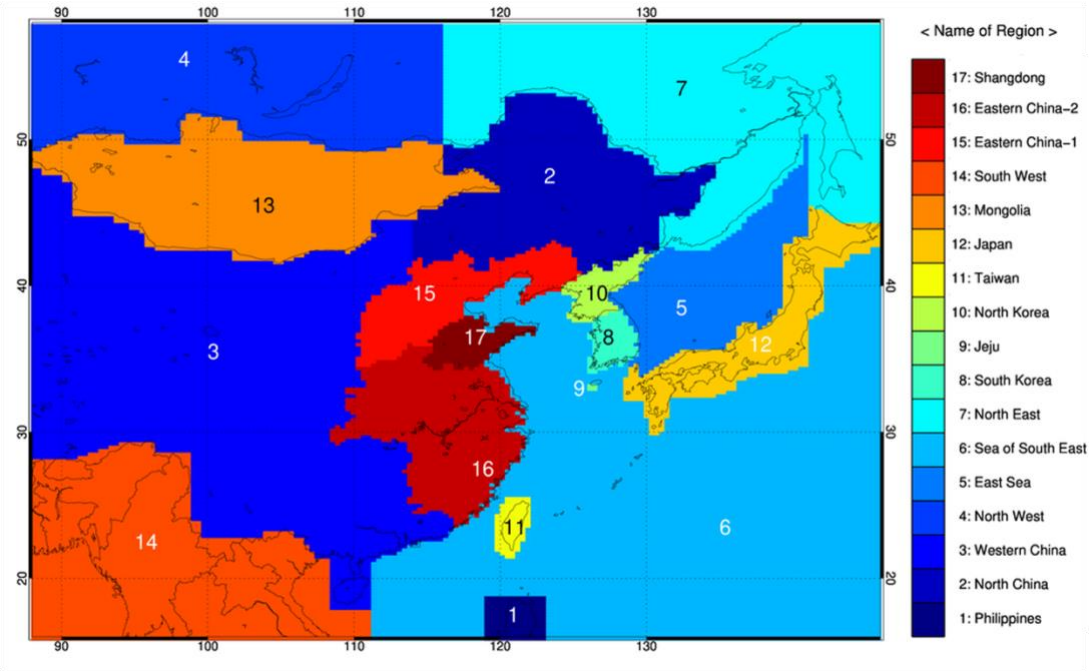

Figure S2a: The division of East Asia into 17 named potential source regions.

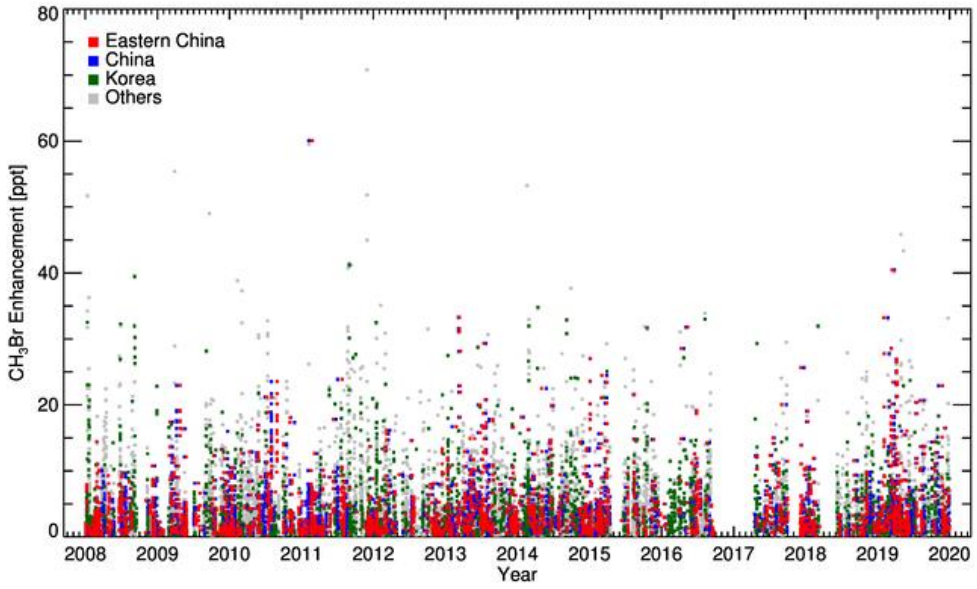

Figure S2b: The time series of enhancement of CH_3Br above baseline for 2008-2019; the aggregated air-mass regional origins are shown as red (eastern China), blue (China), green (Korea), and others (grey), respectively.

Fig. S2a shows the 17-potential source regions for East Asia. The regional origin of an air-mass that inflows to Gosan is classified from the backward trajectory analysis using HYSPLIT. In this study, the aggregated source regions were designated as China (2, 3, 15, 16 and 17), eastern China (15, 16 and 17), Korea (8, 9 and 10) and the remining regions were classified as others (as shown in Fig. S2b). Eastern China-1 consists of Beijing, Liaoning, Tianjin, Hebei and Shanxi provinces, while eastern China-2 consists of Henan, Hubei, Anhui, Jiangsu, Shanghai, Jiangxi, Zhejiang and Fujian provinces.

Fig. S2b is the time series of CH_3Br enhancements (pollution – baseline) for the same period as shown in Fig. 2 of the main manuscript; the regional origin of each air mass is indicated by colour with regards to the 17 regions (Fig S2a), aggregated to eastern China, China, Korea and others.

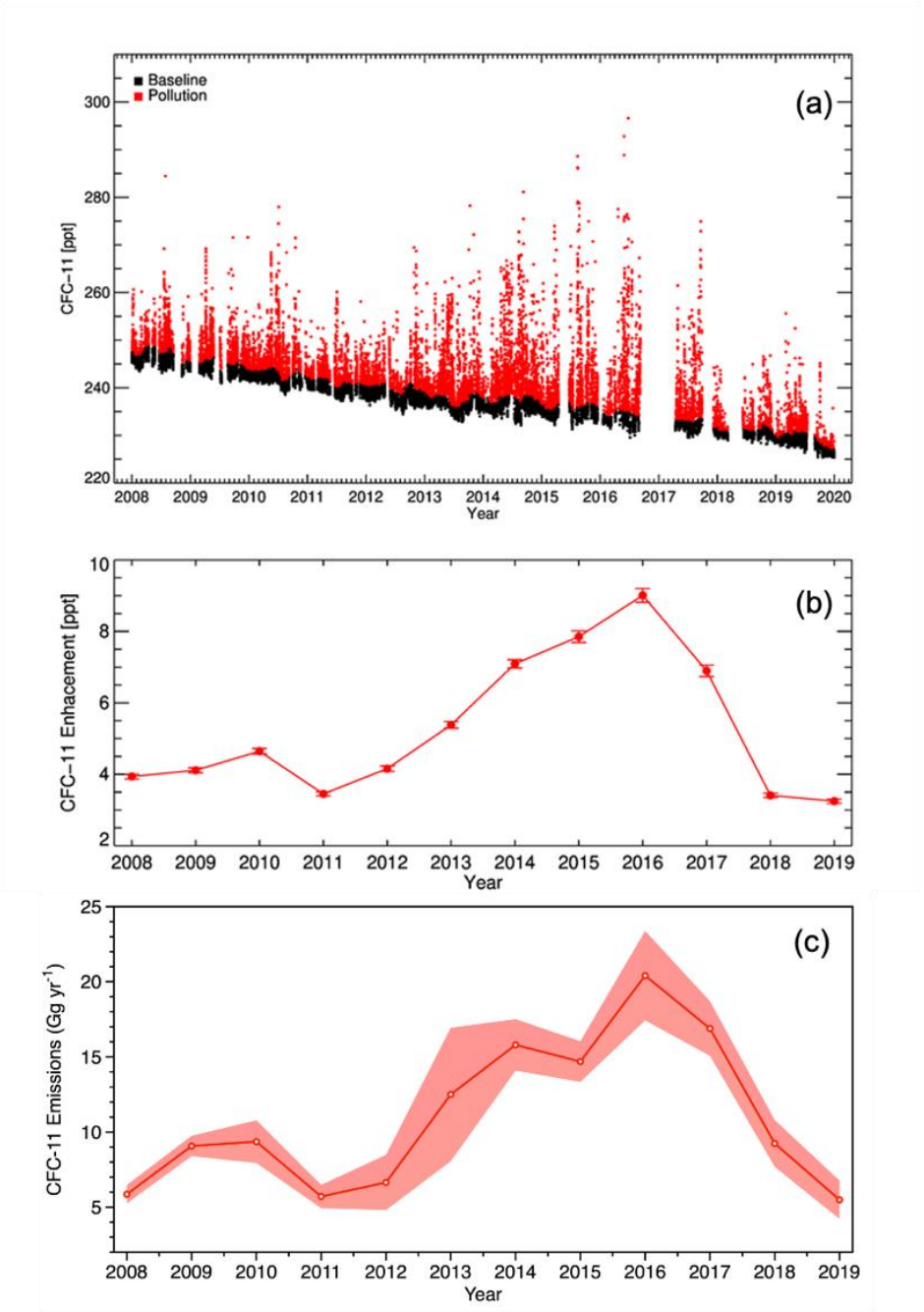

Figure S3: (a) Concentration of CFC-11 in the atmosphere observed at Gosan in the period 2008–2019; the baseline data are shown in black determined by a statistical filtering method (O'Doherty et al., 2001); the polluted data (elevated above the baseline data) are shown in red. (b) The time series for the annual average of enhancement of CFC-11 above baseline; the error bars denote the standard error of the mean (there are typically 175 data points per annual mean). (c) Annual mean and standard deviation of CFC-11 emissions for eastern China that estimated by 4-independent inversion frameworks (Park et al., 2021).

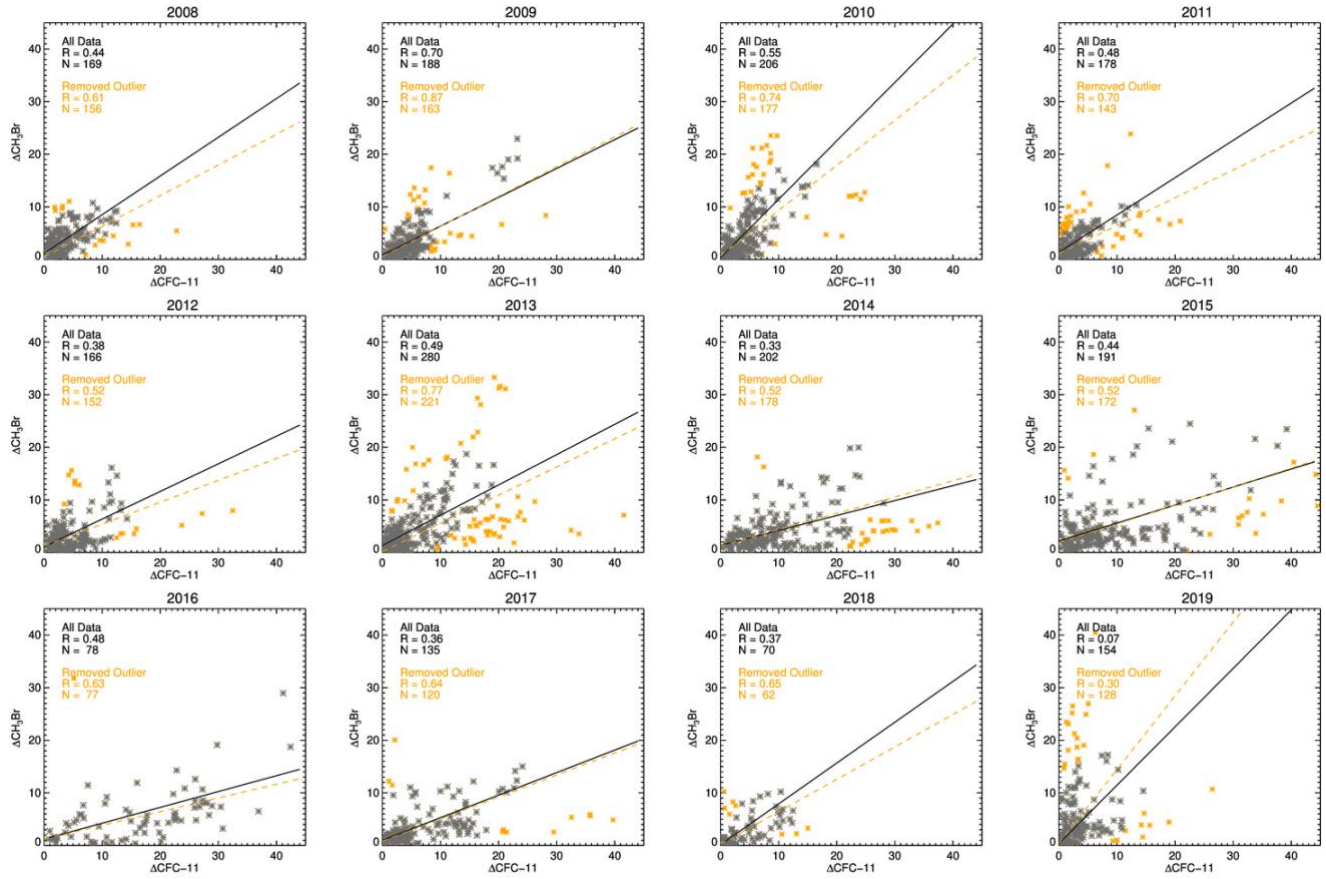

Figure S4: The annual correlation between the enhancement of CH_3Br and CFC-11 above baseline measured at Gosan from 2008 to 2019. The weighted Deming regressions were applied for all data (which represented in Fig. 7 of main text; black) and removed outlier data (yellow). The yellow asterisks correspond to observations that were considered outliers and removed.

Figure S4 shows the xy plot of the annual enhancements of CH_3Br and CFC-11 above baseline for all data (black) and data with outliers removed (yellow). To filter out outliers, we selected data in the range of Q1-1.5*IQR < the difference of CH_3Br and CFC-11 < Q3+1.5*IQR (outliers removed). The linear regression between the two pollutants were derived from the weighted Deming regression (WDR) method suggested (Wu and Yu, 2018). As described in Table S1, the estimated annual slopes and uncertainties between CH_3Br and CFC-11 by WDR does not differ significantly with or without outliers. This demonstrated the robust WDR that can cover the overall scatter trend well.

Table S1: Annual slopes and their uncertainties between ΔCH_3Br and ΔCFC-11 as shown in Figure S4. The annual median values for individual ratios ($\Delta CH_3Br/\Delta$CFC-11) along with 16th and 84th percentile ranges.

Year	CH_3Br *vs.* CFC-11				
	All Data		Removed Outlier		Ratio ($\Delta CH_3Br/\Delta$CFC-11)
	Slope	Uncertainty of slope	Slope	Uncertainty of slope	Median (16th – 84th percentile)
2008	0.74	0.18	0.64	0.19	0.89 (0.39 – 2.55)
2009	0.55	0.09	0.58	0.06	0.68 (0.31 – 1.47)
2010	1.10	0.12	0.94	0.16	1.12 (0.44 – 2.25)
2011	0.71	0.12	0.62	0.12	0.96 (0.39 – 2.98)
2012	0.53	0.25	0.45	0.27	0.66 (0.24 – 1.62)
2013	0.58	0.07	0.59	0.09	0.78 (0.27 – 1.66)
2014	0.28	0.04	0.29	0.05	0.38 (0.14 – 0.92)
2015	0.34	0.13	0.38	0.14	0.46 (0.22 – 1.53)
2016	0.30	0.07	0.26	0.04	0.29 (0.11 – 0.85)
2017	0.43	0.09	0.43	0.08	0.47 (0.20 – 1.27)
2018	0.77	0.11	0.70	0.10	0.65 (0.26 – 1.70)
2019*	1.10	0.12	0.94	0.16	1.40 (0.37 – 4.79)

* Note: slope and uncertainty for 2019 used 2010 values.

Table S2: Global CH_3Br emissions for QPS and non-QPS from 2008 to 2019 (data available at Ozone Secretariat website, http://ozone.unep.org).

Year	UNEP reported (Gg yr^{-1})	
	QPS	non-QPS
2008	7.38	6.85
2009	7.67	5.74
2010	9.20	4.95
2011	8.15	3.14
2012	7.44	2.27
2013	8.25	1.56
2014	9.34	0.69
2015	6.87	0.35
2016	7.01	0.61
2017	8.32	0.23
2018	8.97	0.00
2019*	7.53	0.01

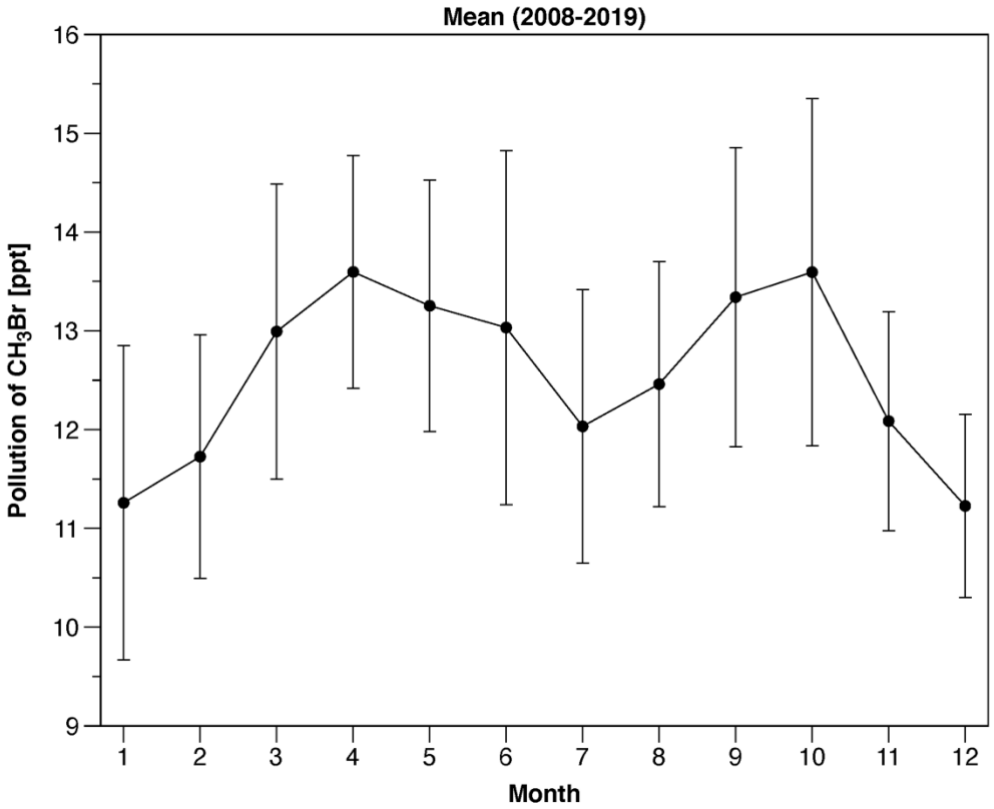

Figure S5: Monthly mean of polluted concentrations of CH_3Br at Gosan from 2008 to 2019. Error bars represent the standard deviation of each month.

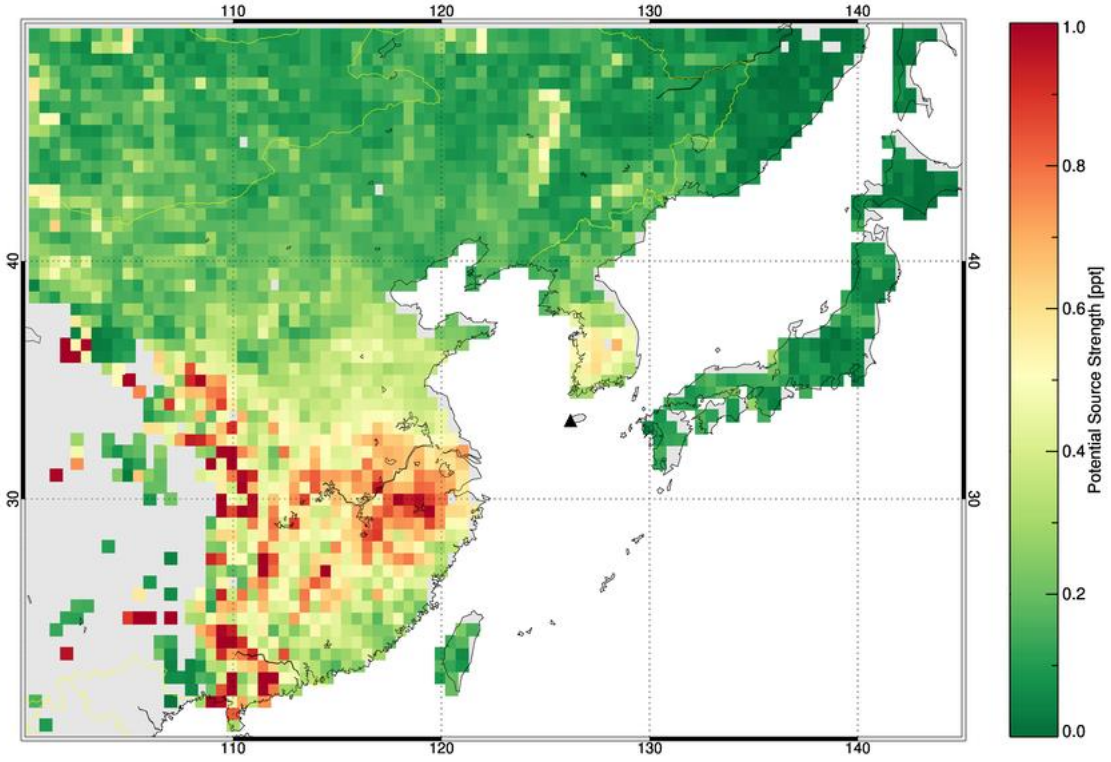

Figure S6: Potential source regions derived from back-trajectory analyses of SO_2F_2 pollution data at Gosan from 2008 to 2019. The location of Gosan station is represented as a black triangle.

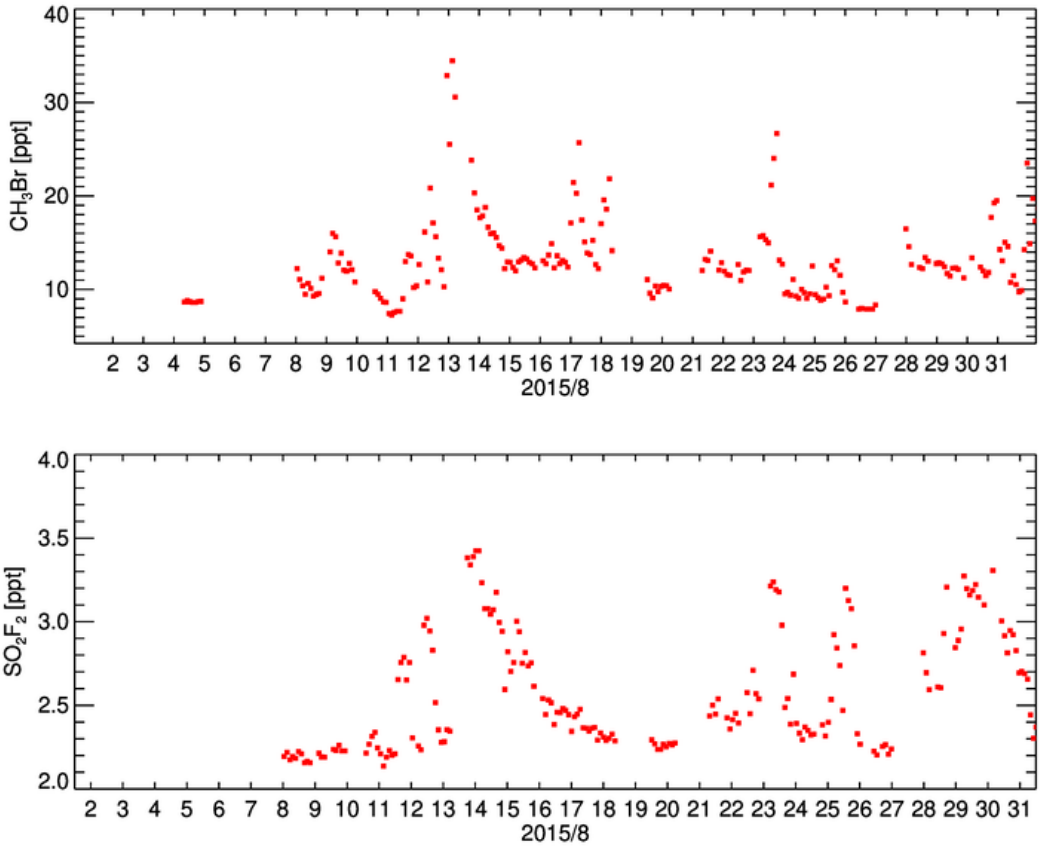

Figure S7: Observed concentrations of CH_3Br and SO_2F_2 at Gosan during August 2015; note the correlated and non-correlated pollution events.

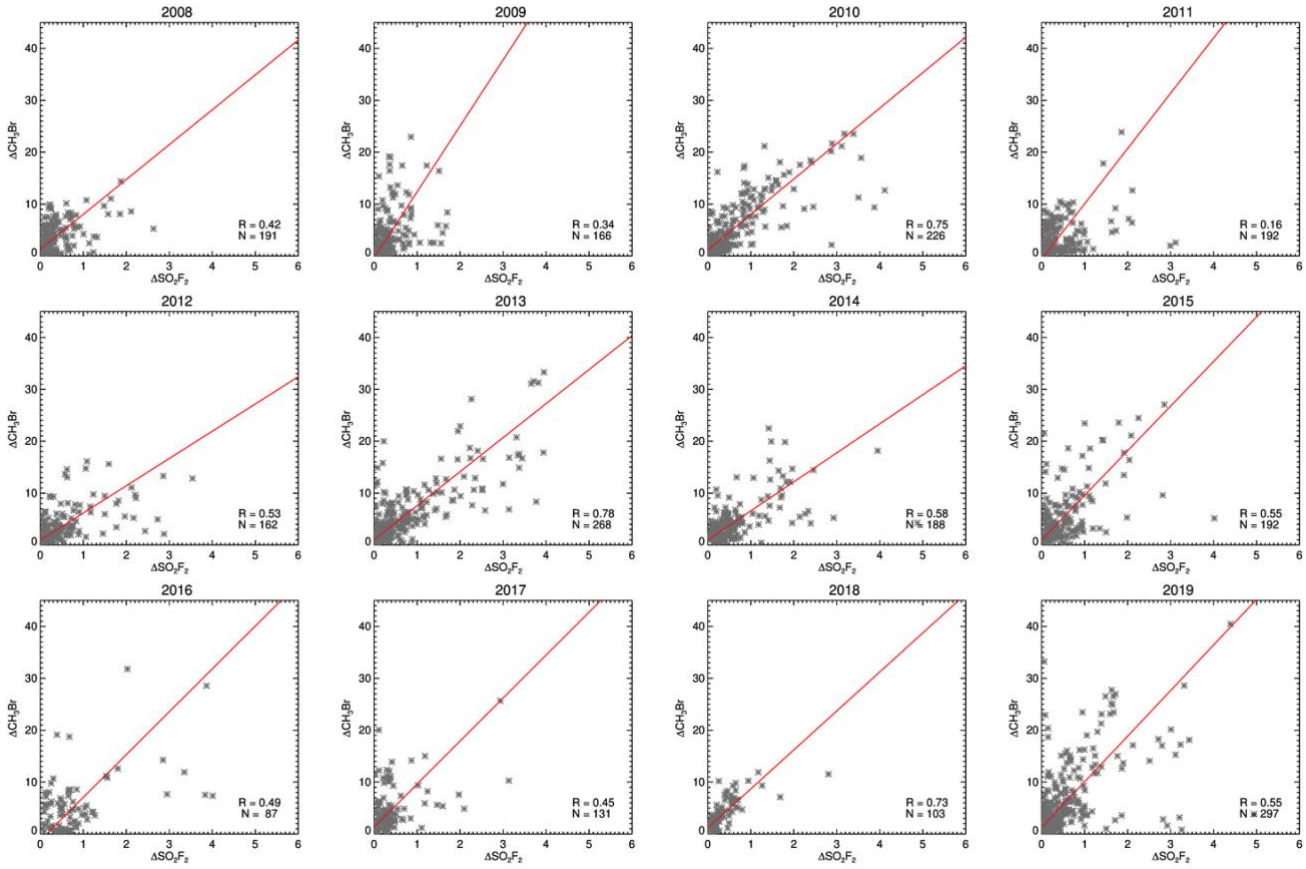

Figure S8: Same as Figure S4, but for CH_3Br and SO_2F_2.

Table S3: Same as Table S1, but for CH_3Br and SO_2F_2 as shown in Figure S8, and annual SO_2F_2 emissions and estimated CH_3Br emissions for post-harvest treatment by ISC method. The post-harvest treatment SO_2F_2 emissions were derived for eastern China from the global emission data of Gressent et al., 2021.

Year	CH_3Br *vs.* SO_2F_2		SO_2F_2 emissions (from Gressent et al., 2021) ($Gg\ yr^{-1}$)	CH_3Br emissions for post-harvest treatment ($Gg\ yr^{-1}$)
	Slope	Uncertainty of slope		
2008	6.71	1.27	-	-
2009	12.70	3.39	-	-
2010	6.83	0.43	-	-
2011	10.65	6.26	-	-
2012	5.25	0.75	-	-
2013	6.56	0.34	-	-
2014	5.60	0.65	0.13	0.7 ± 0.1
2015	8.60	1.07	0.12	1.0 ± 0.1
2016	8.25	1.81	0.13	1.0 ± 0.2
2017	8.28	1.71	0.13	1.0 ± 0.2
2018	7.51	0.74	0.13	0.9 ± 0.1
2019	8.78	0.88	0.13	1.1 ± 0.1

SI. References

Li, S., Kim, J., Park, S., Kim, S. K., Park, M. K., Mühle, J., Lee, G., Lee, M., Jo, C. O. and Kim, K. R.: Source identification and apportionment of halogenated compounds observed at a remote site in East Asia, Environ. Sci. Technol., doi:10.1021/es402776w, 2014.

O'Doherty, S., Simmonds, P. G., Cunnold, D. M., Wang, H. J., Sturrock, G. A., Fraser, P. J., Ryall, D., Derwent, R. G., Weiss, R. F., Salameh, P., Miller, B. R. and Prinn, R. G.: In situ chloroform measurements at Advanced Global Atmospheric Gases Experiment atmospheric research stations from 1994 to 1998, J. Geophys. Res. Atmos., doi:10.1029/2000JD900792, 2001.

Park, S., Western, L. M., Saito, T., Redington, A. L., Henne, S., Fang, X., Prinn, R. G., Manning, A. J., Montzka, S. A., Fraser, P. J., Ganesan, A. L., Harth, C. M., Kim, J., Krummel, P. B., Liang, Q., Mühle, J., O'Doherty, S., Park, H., Park, M.-K., Reimann, S., Salameh, P. K., Weiss, R. F. and Rigby, M.: A decline in emissions of CFC-11 and related chemicals from eastern China, Nature, doi:10.1038/s41586-021-03277-w, 2021.

Poirot, R. L. and Wishinski, P. R.: Visibility, sulfate and air mass history associated with the summertime aerosol in northern Vermont, Atmos. Environ., doi:10.1016/0004-6981(86)90018-1, 1986.

Reimann, S., Schaub, D., Stemmler, K., Folini, D., Hill, M., Hofer, P., Buchmann, B., Simmonds, P. G., Greally, B. R. and O'Doherty, S.: Halogenated greenhouse gases at the Swiss High Alpine Site of Jungfraujoch (3580 m asl): Continuous measurements and their use for regional European source allocation, J. Geophys. Res. Atmos., doi:10.1029/2003jd003923, 2004.

Seibert, P., Kromp-Kolb, H., Baltensperger, U., Jost, D. T. and Schwikowski, M.: Trajectory Analysis of High-Alpine Air Pollution Data, in Air Pollution Modeling and Its Application X., 1994.

Wu, C. and Zhen Yu, J.: Evaluation of linear regression techniques for atmospheric applications: The importance of appropriate weighting, Atmos. Meas. Tech., doi:10.5194/amt-11-1233-2018, 2018.